Oil & Natural Gas Technology

DOE Award No.: DE-FC26-06NT43067

Compute gas/water interface geometry within fracture (Task 5.3 Technical Report)

Mechanisms Leading to Co-Existence of Gas and Hydrate in Ocean Sediments

Submitted by:
The University of Texas at Austin
1 University Station C0300
Austin, TX 78712-0228

Prepared for:
United States Department of Energy
National Energy Technology Laboratory

October 24, 2008

Office of Fossil Energy

MECHANISMS LEADING TO CO-EXISTENCE OF GAS AND HYDRATE IN OCEAN SEDIMENTS

CONTRACT NO. DE-FC26-06NT43067

Deliverable 5.3:
Report on Task 5.3: Compute gas/water interface geometry within fracture

October 30, 2008

Prepared by

Steven L. Bryant
Maša Prodanović
Department of Petroleum and Geosystems Engineering
The University of Texas at Austin
1 University Station C0300
Austin, TX 78712-0228
Phone: (512) 471 3250
Email: steven_bryant@mail.utexas.edu

Prepared for
U.S. Department of Energy - NETL
3610 Collins Ferry Road
P.O. Box 880
Morgantown, WV 26508

Objective of Task 5.3

In the conceptual model to be examined in this project, hydrate formation depends upon the location and geometry of the gas/water interface. The gas/water interface in turn depends on the competition between capillarity-controlled meniscus movement (drainage and imbibition) and grain-mechanics-controlled sediment displacement (sediment fracturing). To study this competition, we have computed gas/water interface geometry within a fracture for representative stages of fracture propagation from Task 4. We have also applied the level set method to compute the capillary-controlled configuration of gas and water in rough-walled fractures. We also applied the model of capillarity-controlled displacement in a fracture domain that is bounded by model sediments. This yields insight into the magnitude of drainage of methane from the fracture into different model sediments.

Description of Findings in Task 5.3

Gas/water Interface Movement in Rough-walled Fractures

We have investigated of the capillary-controlled configuration of gas and water in the rough-walled fractures using progressive quasi-static (PQS) algorithm. Compared to our earlier efforts, we validated the model using available pore scale experiments and extended the method to account for trapping of gas (non-wetting) phase. We summarize main results on two examples of three-dimensional fractures (see below).

1) **Fractured Berea sandstone.** This fracture comes from the experiment done by Dr. Zuleima Karpyn of Pennsylvania State University and enables us to visually compare the level set method drainage and imbibition results with an actual experiment.
2) **Simulation in fractured sediment model.** We artificially created a fracture in mono-disperse sphere packing (resembling a fracture opened by methane gas) and observed very different residual fluid configurations for different directions of the displacement.

Fractured Berea Sandstone

We used an upscaled version of 389 × 116 × 25 elements of the original CT image from Z. Karpyn in order to compare our simulations with experiments. The computational domain thus corresponds to a 101 × 25 × 5.5 mm^3 physical domain.

The LSMPQS simulations agree generally with the experiment. Fig. 1 shows the fracture aperture field (Fig. 1a) and the experimentally determined drainage endpoint (Fig 1b). The nonwetting phase (oil) accessed the fracture from one end (bottom of image), displacing wetting phase (brine) from the other end (top of image). As seen in Fig. 1c, oil (non-wetting phase) at the LSMPQS simulation drainage endpoint occupies wider spaces and cannot enter regions of small aperture.

There are discrepancies in some details of the configuration. One reason is likely to be the upscaling of the aperture field for the simulation. Some of the detailed structure that

controls meniscus movement was averaged out in the simulation domain. Another is that the simulation uses a contact angle of zero, but the contact angle of the experimental fluids was estimated to be 15° for drainage and 25° for imbibition. Finally, the oil configuration in Fig. 1b is the result of segmentation of a multiphase image. Segmentation of such images is prone to misidentification errors: a subjective choice must be made regarding the range of gray scale values corresponding to each phase; different choices for the endpoints of these ranges can affect the interpreted location of the phases.

Selected fluid configurations for drainage simulation are shown in Figs. 2. Bottom (inlet) and top (outlet) are the only boundaries open to flow. Figures 2b and 2c show both oil and water configuration for the same capillary pressure. Water surrounds asperities (visible as white breaks in the green water surface), and is mostly in blobs disconnected from the inlet and outlet but is assumed to flow via water films. We used oil-water interfacial tension value $\sigma_{ow} = 41.2 \cdot 10^{-3}\ N/m$ in order to scale the curvatures from LSMPQS simulation to capillary pressure values. Figure 3b shows the predicted capillary pressure – saturation relationship during drainage and imbibition. Unfortunately no experimental data on capillary pressure curve are available.

Figure 4 shows oil configuration for various imbibition stages. We identify and record the trapped oil blobs (i.e. disconnected from both the main oil phase and the open flow boundaries). Pressure typically needs to be substantially reduced before the trapped phase is observed. The first instance we observe is at $P_{23} = 236.1\ Pa$ (subscript 23 denotes the discrete simulation step) and Fig. 4b shows a slightly later configuration that already has seven trapped oil blobs (in blue). Figure 4c shows one more step until the last imbibition stage shown in Fig. 4d where all oil present is trapped (and thus the imbibition simulation stops).

We conclude that the LSMPQS algorithm successfully captures the physics of capillarity-controlled displacements in rough-walled fractures. This constitutes a significant advance over previously available aperture-scale simulations. Several authors have reported network models of displacement within fractures, but most required *ad hoc* assumptions to construct the network and none accounted rigorously for the in-plane radius of curvature of the meniscus. The results shown above are the first to make no simplifications of the physics of displacement. The simulated disconnection and trapping of the nonwetting phase is especially noteworthy, as it occurs spontaneously within the simulation. The behavior is consistent with our earlier results using this method to study imbibition in granular materials, which agree well with experiments.

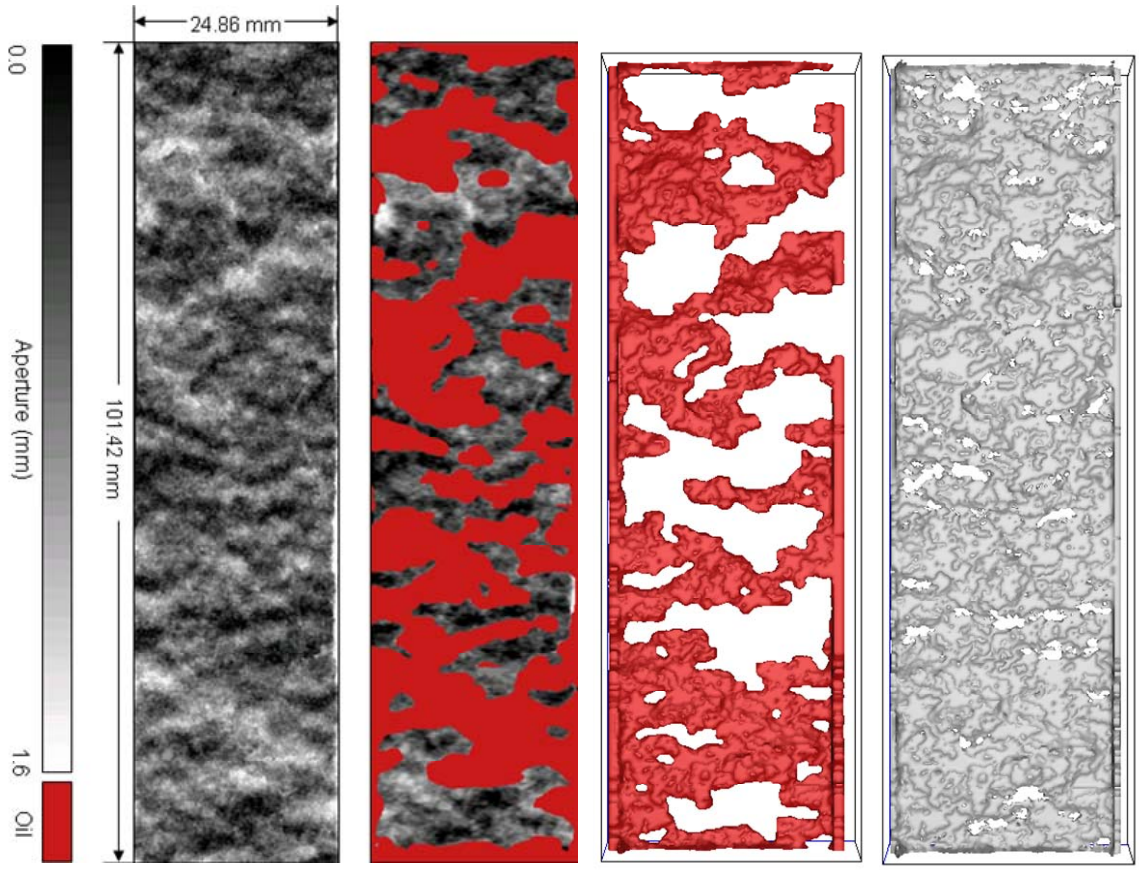

(a) (b) (c) (d)

Fig. 1—Visual comparison of the Berea fracture experimental data (from Z. Karpyn) and LSMPQS simulation. (a) Fracture aperture field shown in shades of gray. Asperities (contact points) are where the aperture field is black and wide parts are where the aperture data is white/light gray. (b) Oil configuration (green) inferred from CT image at the drainage endpoint (S_w=0.35) overlaid upon the aperture field information (grayscale). (c) Top view of the oil configuration from LSMPQS drainage simulation at S_w=0.28. (d) Top view of the pore-grain interface used in LSMPQS simulation. White breaks correspond to asperities.

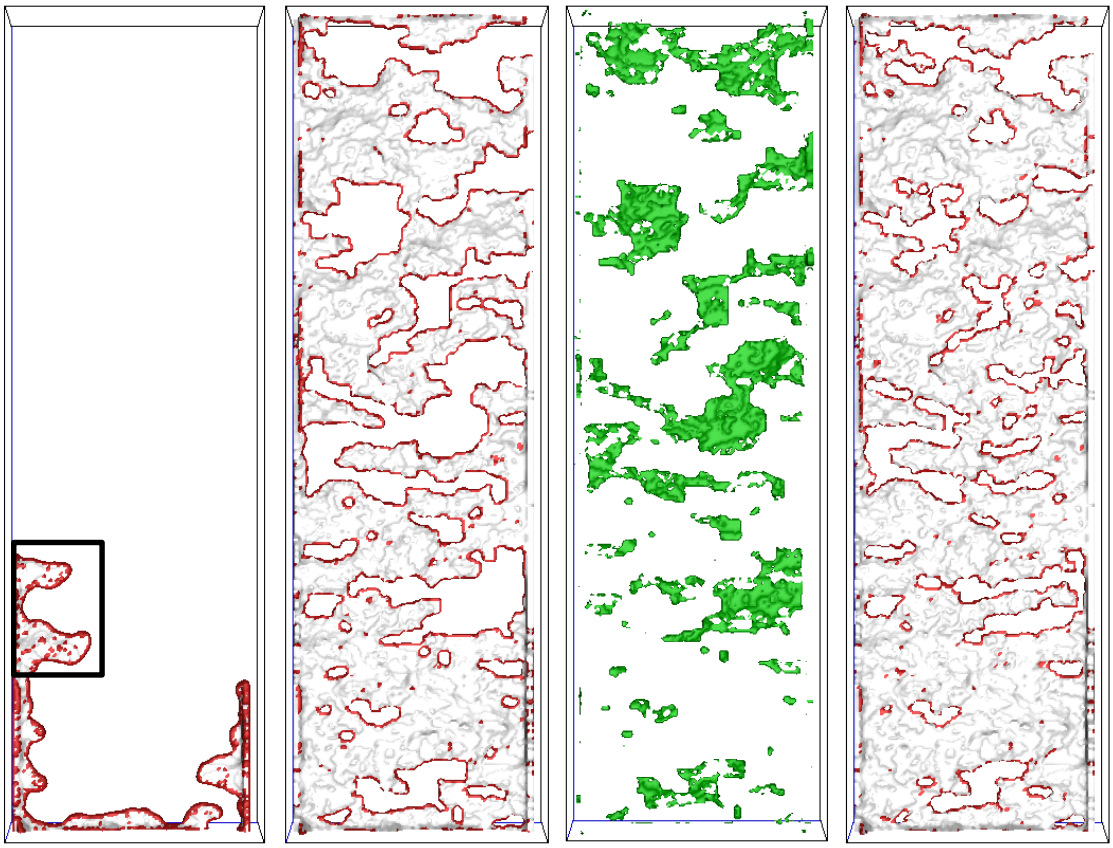

(a) (b) (c) (d)

Fig. 2—(a) Non-wetting phase surface at drainage capillary pressure $P_2 = 153.7\ Pa$. The fluid-fluid interface is shown in red, and the non-wetting phase/grain interface is shown in gray. Long red strip in fracture plane is the main meniscus, small red patches represent the meniscus trying to get into nooks in the grain surface. See Fig 3a for an enlarged view of the region within the black rectangle. (b) Non-wetting phase interface at drainage capillary pressure $P_{13} = 606.9\ Pa$. (c) Wetting fluid interface (in green) at the same pressure stage as in b. (d) Non-wetting phase interface at the end of simulation, $P_{26} = 1142.5\ Pa$.

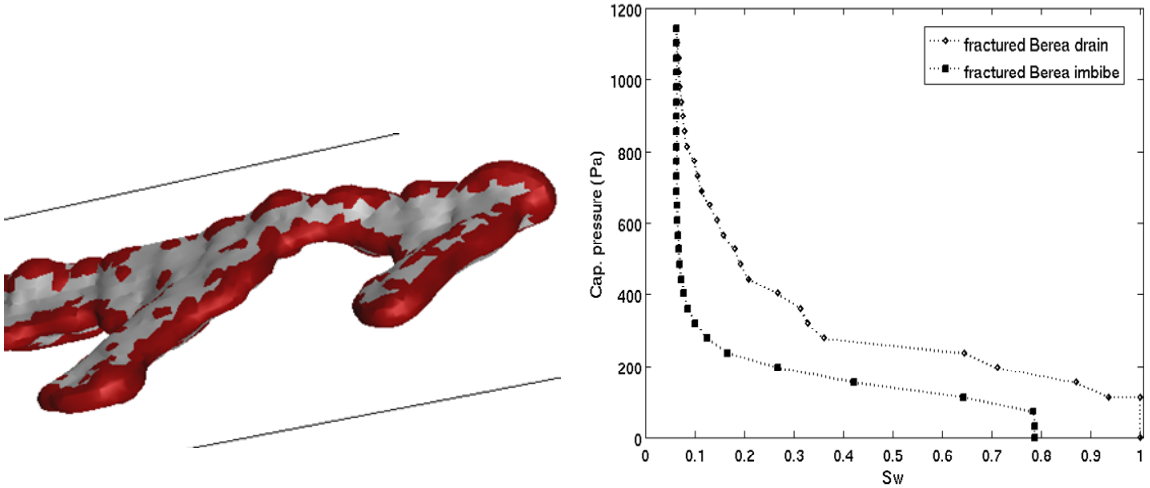

(a) (b)

Fig. 3—(a) Non-wetting phase interface detail corresponding to outlined area from Fig 2a. Long red strip in fracture plane is the main meniscus, small red patches represent the meniscus trying to get into nooks in the grain surface. (b) Simulated capillary pressure – saturation curve for drainage and imbibition in fractured Berea.

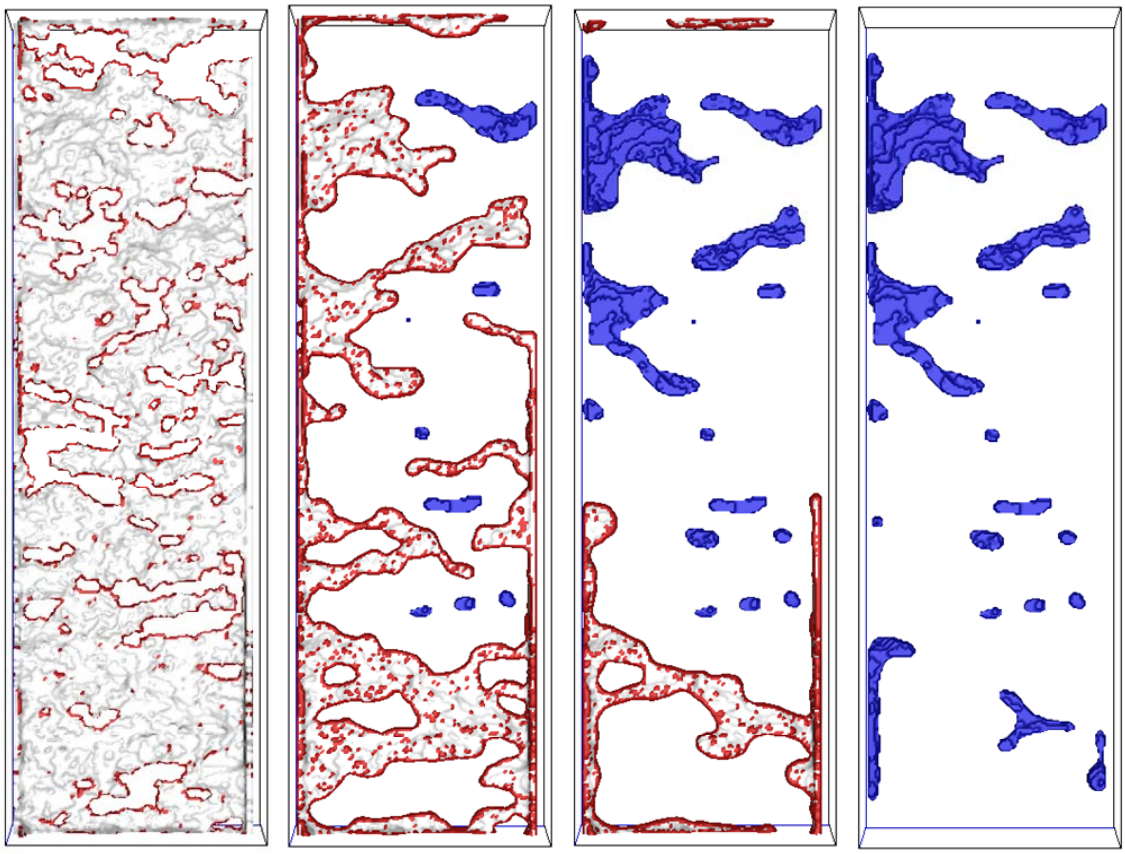

Fig. 4—Oil surface for various imbibition stages. Gray is oil-grain surface, red is oil-water interface for the main connected component of oil and disconnected (residual) oil interface is shown in blue. (a) $P_9^{imb} = 812.9\ Pa$. (b) $P_{25}^{imb} = 153.7\ Pa$. (c) $P_{26}^{imb} = 112.5\ Pa$. (d) Final imbibition configuration for $P_{28}^{imb} = 30.1\ Pa$ consists only of residual oil blobs (volume fraction of 0.214).

Fractured Sediment Model

A subset of a dense, random packing of equal spheres (radius $R = 1$) measured by Finney (1970) was artificially fractured by moving spheres away from and perpendicular to a z-plane. We kept ten randomly chosen pairs of spheres in contact (see Fig. 5a) since the contact points play important role in final fluid configurations. We then performed drainage and imbibition with two different boundary conditions. In one case, the invading (gas) phase entered the domain in the direction parallel to the z-plane of the fracture. It thus had access to fracture and matrix simultaneously. In the other, the gas phase entered the domain in the direction perpendicular to the fracture plane. It had access only to the matrix initially. Invasion of the fracture could occur only from the matrix. The fracture and associated matrix occupied a volume of $[-8R, 8R]^3$ discretized into a mesh of 160^3 numerical cells.

Figure 5b shows gas configuration at a stage that essentially occupied entire fracture opening. At a later drainage step shown in Fig. 6a, drainage of the adjoining matrix has begun. We plot drainage and imbibition curvature-saturation curves in two ways: one measuring saturation in the entire volume and the other set measuring saturation in the matrix adjoining the fracture only (Fig 6b). The "matrix only" drainage curve does not show a sharp percolation threshold (the threshold is at $\kappa = 6$ for monodisperse spheres (Behseresht *et al*. 2007)) because the gas accesses the volume from the entire fracture face. The fracture volume was inferred from the non-wetting fluid configuration shown in Fig. 5b, and subtracted from the overall volume to get the matrix pore space. Imbibition configurations are shown in Figs. 10. Note the disconnected blobs of non-wetting phase result from specifically checking for and recording trapped (disconnected) phase during imbibition simulation.

We repeat the simulation sequence for rotated geometry where the displacement direction is perpendicular to the fracture plane. That is, the fluids access the fracture only from the matrix. This proves to have a major influence. The capillary pressure curve is different for each displacement direction, but more significantly, the saturation and location of the residual nonwetting phase is very different (see Fig. 8). All the nonwetting phase occupying the fracture is trapped.

We conclude that the LSMPQS method successfully captures the physics of capillarity-controlled displacements within a fracture bounded by a granular matrix. This situation is of immediate relevance to gas/water displacements within the hydrate stability zone. The method correctly identifies a two-scale pressure-saturation curve when gas can access both the fracture and the matrix simultaneously: the fracture drains at small pressures, with subsequent invasion of the matrix at large pressures. Trapping of gas in the fracture depends entirely on whether the fracture is connected to a large reservoir of gas. If that connection is lost, then large saturations of gas will be trapped in the fracture. This is likely to affect the growth habit of hydrate.

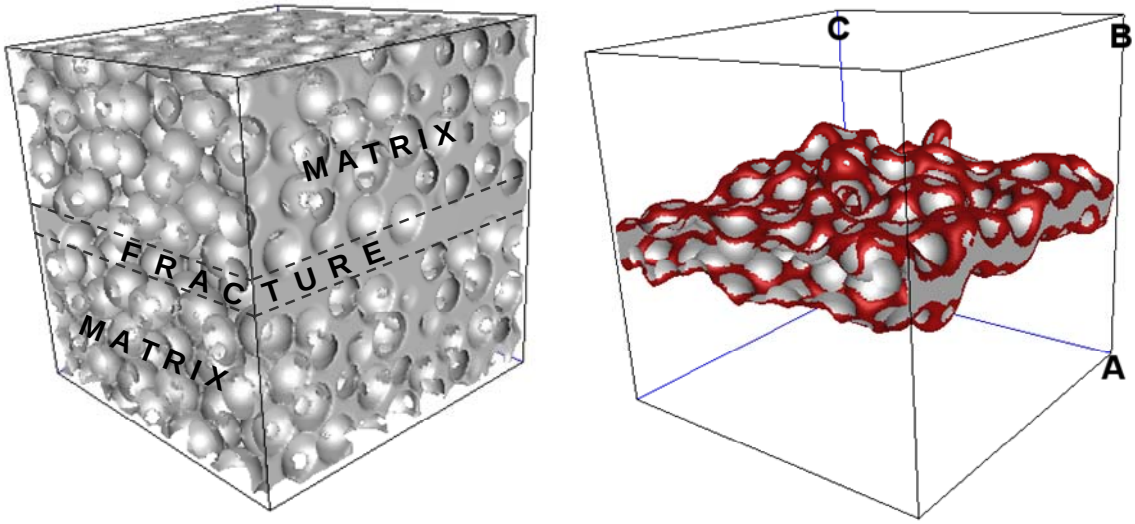

(a) (b)

Fig. 5—(a) Grain surface for fractured sphere pack. Fracture position can be inferred from the flat portion of sealed volume on the side. (b) Drainage simulatioin starts from the face marked ABC. Non-wetting fluid (gas) surface is shown in red at curvature $C_3 = 2.9$ at the drainage step where the entire fracture opening is filled with gas (and capillary invasion into the matrix has just started).

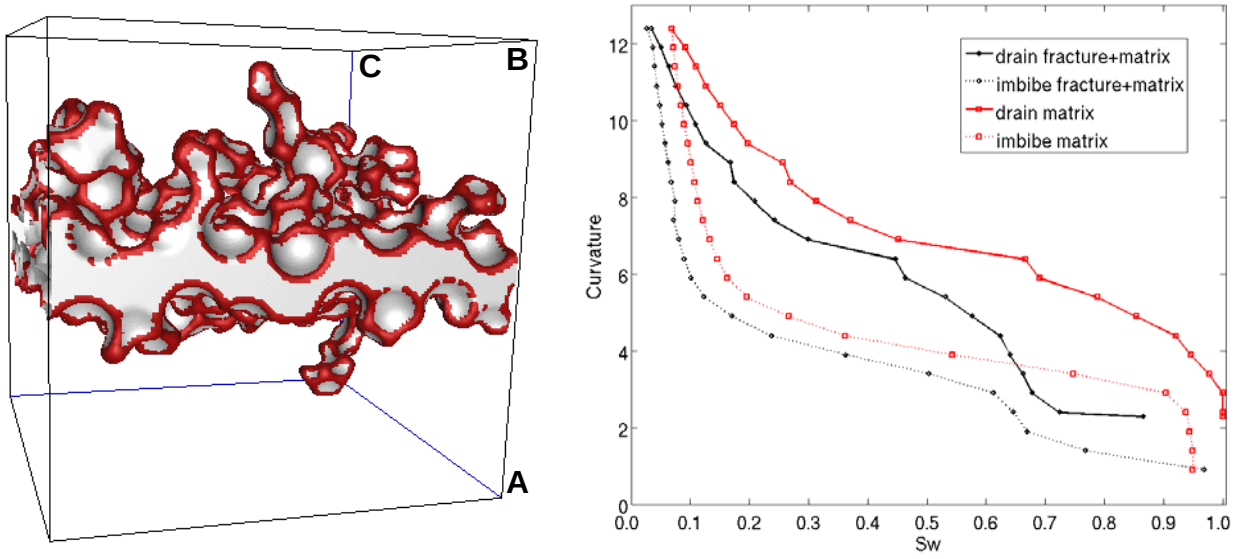

(a) (b)

Fig. 6—(a) Side view of gas (non-wetting fluid) at drainage for $C_7 = 4.9$ when the gas phase started moving from the fracture into the matrix. It entered the domain from the face marked ABC, so the fracture drains first at a curvature of about 2.2. (b) Curvature vs. wetting fluid saturation plots for drainage and imbibition in fractured sphere pack. Curves labeled 'fracture+matrix' show saturation in entire volume, whereas curves labeled 'matrix' show saturation in the matrix adjoining the fracture only.

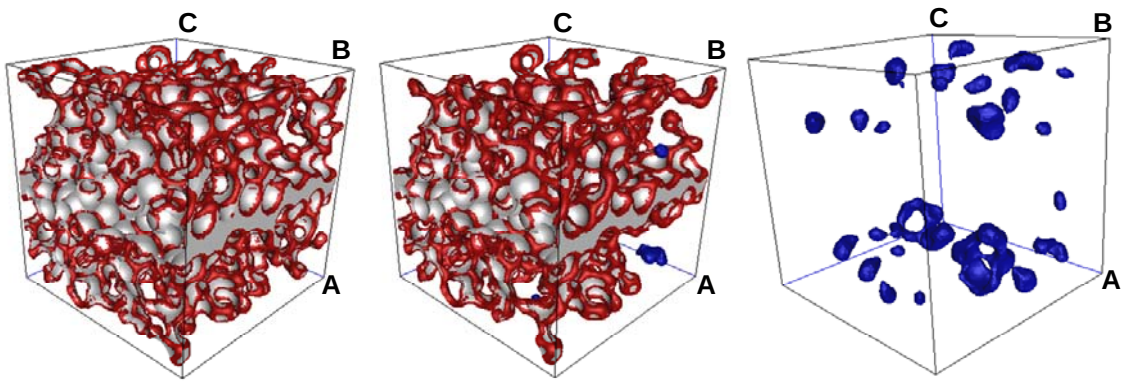

(a) (b) (c)

Fig. 7—NW phase (gas) imbibition configurations for fractured sphere pack. The wetting phase (brine) enters the domain in the direction parallel to the fracture from from the face marked ABC, and gas can exit through the face directly across from the entry face. Disconnected gas blobs are shown in blue and the gas connected to the inlet/outlet is shown in red/gray (red is fluid meniscus, gray is contact with grain). From left to right are shown imbibition steps at curvatures $C_{17}^i = 4.4$, $C_{18}^i = 3.4$, and $C_{24}^i = 0.4$ (final, all of the gas is in disconnected form).

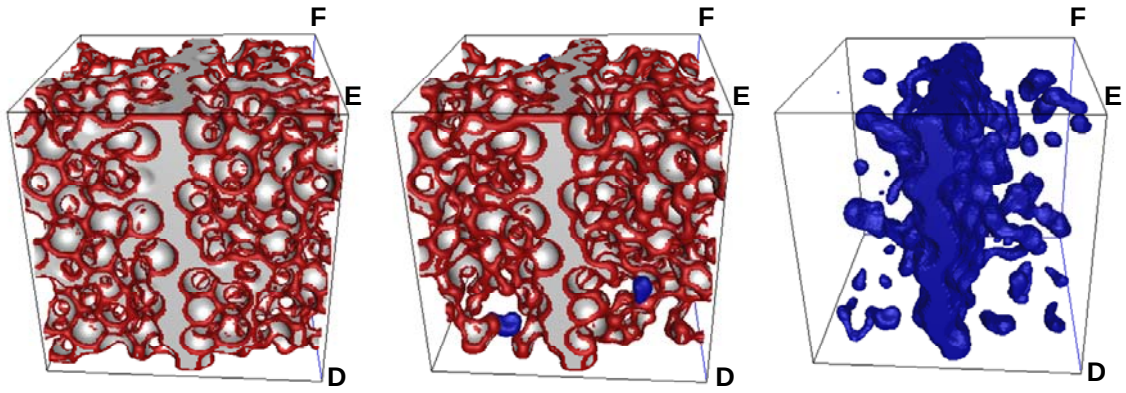

(a) (b) (c)

Fig. 8—NW fluid (gas) imbibition configurations for steps (a) $C_8^i = 5.15$, (b) $C_9^i = 4.15$ and (c) $C_8^i = 2.15$ (final) for rotated geometry. The image is oriented so that the gas in fracture is viewed properly (during drainage the nonwetting phase went from the face marked DEF on the right to the left – the two opposite faces are the only ones open to flow). At the final imbibition step the entire fracture is filled with trapped gas.

National Energy Technology Laboratory

626 Cochrans Mill Road
P.O. Box 10940
Pittsburgh, PA 15236-0940

3610 Collins Ferry Road
P.O. Box 880
Morgantown, WV 26507-0880

One West Third Street, Suite 1400
Tulsa, OK 74103-3519

1450 Queen Avenue SW
Albany, OR 97321-2198

2175 University Ave. South
Suite 201
Fairbanks, AK 99709

Visit the NETL website at:
www.netl.doe.gov

Customer Service:
1-800-553-7681